

Natural Convection Heat Transfer of A Straight-fin Heat Sink

Xiangrui Meng^{1,2}, Jie Zhu^{2,*}, Xinli Wei^{1,*}, Yuying Yan²

¹ School of Chemical Engineering and Energy, Zhengzhou University, Henan, China

² Department of Architecture and Built Environment, The University of Nottingham,
Nottingham, UK

ABSTRACT

The influence of mounting angle on heat dissipation performance of a heat sink under natural convection condition is investigated in this paper by numerical simulation and experimental test. It is found that the heat sink achieves the highest cooling power when its mounting angle is 90 °, while it reaches the lowest when the mounting angle is 15 °, which is 6.88% lower than that of 90 °. A heat transfer stagnation zone is the main factor that affects the cooling power of the heat sink, and its location and area vary with the mounting angle. It is identified that cutting the heat transfer stagnation zone is an effective way to improve the heat sink performance.

Keywords:

Natural Convection Heat Transfer, Heat Sink, Mounting Angle, Stagnation Zone

*Corresponding author. Email address: lazjz@nottingham.ac.uk (J. Zhu), xlwei@zzu.edu.cn (X. Wei).

26 **1. Introduction**

27 Heat sink is a passive heat exchanger that transfers heat generated by an electronic or a
28 mechanical device to a fluid medium, such as air and liquid coolant. Heat dissipation is very
29 important in the modern electronic industry, according to the statistical data, high temperature
30 causes more than 55% failures of electronics [1]. The heat sink is also used in other areas, for
31 example, heat dissipation of DSC (Dye-Sensitized Solar Cell) [2]. The heat sink has different
32 structures, and can be classified into active and passive types. Compared to the active heat sink,
33 the passive heat sink dissipates thermal energy through the nature convection, and usually it is
34 made of aluminium finned radiator, so it has high reliability and low cost characters. The
35 driving force in the passive heat sink is buoyancy force generated by temperature difference.
36 The natural convection of heat sink can be divided into limited and infinite space convections
37 according to the external space.

38 Most of the passive heat sinks have simple structure and low cost characters because of
39 their straight fins. Elenbaas [3] carried out the earliest investigation on natural convective heat
40 dissipation for a parallel fin heat sink, Bodoia and Osterle [4] deduced a theoretical solution of
41 the natural convection heat dissipation for the parallel vertical fin heat sink on the basis of
42 theoretical analysis. Other researchers studied and optimised the geometrical dimensions of
43 parallel fin heat sink, and gave out some formulas for calculating geometrical dimensions [5-
44 11]. Heat dissipation performance of the parallel straight fin heat sink can be improved by
45 increasing air turbulence between the fins, such as arranging staggered cylinders [12], drilling
46 holes on base plate [13], opening slots [14] or drilling holes on the fins [15].

47 The above studies are all conducted with the horizontal or vertical heat sink [16-18],
48 nevertheless, the influence of the heat sink mounting angle on heat dissipation is rarely
49 mentioned. Mehrtash et al. [19] studied the effect of inclination of fin-plate heat sink on heat
50 dissipation by numerical simulation with three-dimensional steady-state natural convection.
51 Based on Mehrtash's research results, Tari et al. [20] developed a Nusselt number formula, and
52 found that the fin spacing is an important parameter affecting heat sink thermal performance
53 [21]. Shen et al. [22] investigated heat dissipation properties of the heat sinks placed in eight
54 different directions, and discovered that the denser the fin arrangement, the more sensitive the
55 directionality. There are two main factors limiting the sink natural convection heat dissipation,
56 one is that the heat transfer direction does not match with natural convection flow, and the other
57 one is that the convection between the fins is blocked.

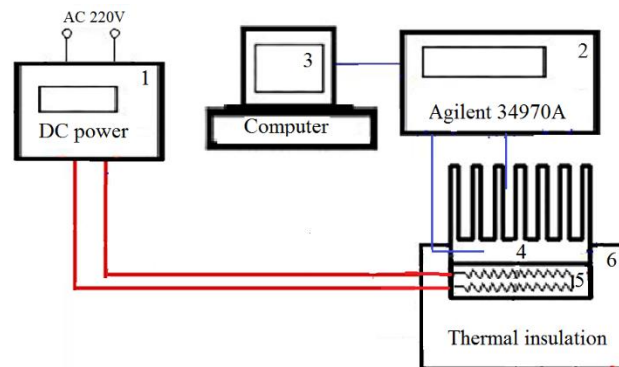
58 In this paper, the influence of heat sink mounting angle on its heat dissipation is
59 investigated. A test rig is designed and built to measure heat dissipation performances of a heat
60 sink at different mounting angles. The numerical simulation of the heat sink performance is
61 carried out, and the simulation results are compared with the experimental data. The optimum
62 mounting angle of the heat sink is obtained, which is useful for heat sink design and installation.

63 **2. Experimental apparatus**

64 *2.1. General description*

65 The main components of the test rig include a JP1505D DC power supply, a DC heating
66 plate, an Agilent 34970A Data Acquisition, a number of K-type thermocouples and PT100
67 RTDs. The schematic of the test rig is shown in Fig. 1. The experimental system is located in

68 a large closed space without the external interference to achieve the heat sink natural
69 convection environment. A special support is designed to ensure the heat sink could rotate 360°
70 freely, as shown in Fig. 2. The heat sink and heating plate are fastened by bolts to reduce the
71 contact thermal resistance and prevent the relative displacement between them. The heating
72 plate is controlled by the JP1505D DC power supply for different heating powers. The
73 maximum output power of the power supply is 750W, its output voltage range is from 0V to
74 150V with accuracy $\pm 0.3V$ and its current range is from 0A to 5A with accuracy $\pm 0.01A$. The
75 electric heating power is constant during the testing, the surface temperature of heat sink is
76 measured and used to judge heat dissipation performance of the heat sink. The lower surface
77 temperature of the heat sink, the better heat dissipation performance. Assuming heat is only
78 dissipated by the heat sink when the temperature of the heat sink substrate became constant,
79 the heat sink performance can be assessed by its surface temperatures.



80
81 **Fig. 1.** Schematic of the test rig: (1) DC power; (2) Agilent 34970A; (3) computer; (4) heat sink; (5) heating
82 plate; (6) thermal insulation

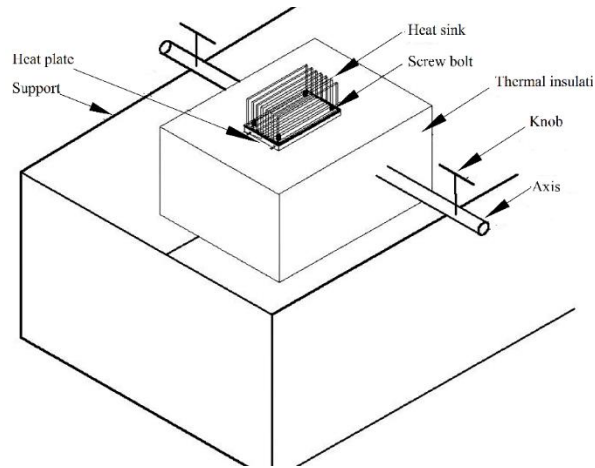
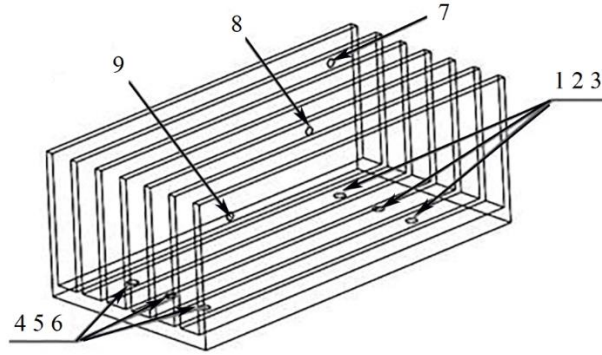


Fig. 2. Schematic of support

83
84

85 The data collection system consists of TC, RTD and Agilent 34970A Data Acquisition,
86 the locations of the measuring points are shown in Fig. 3. TCs are set at Points 1 to 6 to get the
87 heat sink bottom temperatures, RTDs are set at Points 7 to 9 to measure the fin surface
88 temperatures. Agilent 34970A Data Acquisition with module 34902A, which features a built-
89 in thermocouple reference and 16 two-wire channels, has 6 1/2-digit (22-bit) internal DMM
90 and can scan up to 250 channels per second. The K-type armoured thermocouple WRNK-191
91 is used in the experiment. The material of WRNK-191 is nickel-chromium & nickel-silicon
92 and its measurement temperature range is from 0°C to 600°C with accuracy $\pm 0.5^\circ\text{C}$. Because
93 of high thermoelectric power, the WRNK-191 TC has high sensitivity and its thermal response
94 time is 3S. The measurement temperature range of SMD Pt100 RTD Temperature Sensor used
95 for the fin surface is from -50°C to 200°C with accuracy $\pm 0.15^\circ\text{C}$. It can be directly pasted to
96 the fin surface with thermally conductive glue. The tested heat sink is an aluminium straight-
97 fin type, its geometries are listed in Table1.



98
99 **Fig. 3.** Arrangement of measuring points. Points 1-6 K-type thermocouples; Points 7-9, PT100 RTDs

100
101 **Table 1** The geometries of heat sink

Length (mm)	Width (mm)	Base thickness (mm)	Fin height (mm)	Fin thickness (mm)	Fins pitch (mm)	Number of fins
150	76	5	50	3	9.17	7

102 **2.2. Experimental procedure**

- 103 1) Coating thermal grease evenly on the heat sink bottom before fixing it to the heating
104 substrate with screws.
- 105 2) Adjusting the mounting angle of the heat sink to a certain angle, and then checking the
106 output voltage of DC power supply to insure the constant heating power.
- 107 3) The data of each measuring point are to be collected after the heat sink begin to be
108 heated.
- 109 4) The equilibrium between heating and dissipation is reached as the maximum
110 temperature fluctuate on the bottom surface of the heat sink substrate is less than 0.5°C
111 within 20 min.

112 The least thermal resistance method is used to assess the heat sink heat dissipation
113 performance. Thermal resistance R_{th} can be calculated by following equation [5] :

114
$$R_{th} = \frac{T_{ave} - T_{sur}}{Q_{hs}} \quad (1)$$

115 Where T_{ave} and T_{sur} are the average temperatures of the heat plate and the ambient
 116 respectively, Q_{hs} is the heat dissipation power. With constant input power for the heat sink, the
 117 lower the thermal resistance, the higher the heat dissipation ability. Heat transfer coefficient h
 118 of the heat sink can be calculated from the following:

119
$$h = \frac{Q_{hs}}{A \cdot \Delta T} \quad (2)$$

120 Where A is heat sink surface area, ΔT refers to temperature difference between the heat sink
 121 surface and ambient.

122 *2.3. Error Analysis*

123 The experimental errors mainly include systematic and accidental errors. The error δ_y
 124 of a variable y can be obtained by the quadratic equation of the experimental data as the
 125 variables are assumed as $y=f(x_1, x_2, x_3, \dots, x_n)$:

126
$$\delta_y = \sqrt{\left(\frac{\partial y}{\partial x_1}\right)^2 \delta x_1^2 + \left(\frac{\partial y}{\partial x_2}\right)^2 \delta x_2^2 + \dots + \left(\frac{\partial y}{\partial x_n}\right)^2 \delta x_n^2} \quad (3)$$

127 Where, $x_1, x_2, x_3, \dots, x_n$ are independent variables, $\delta x_1, \delta x_2, \delta x_3, \dots, \delta x_n$ are their errors. The
 128 maximum errors of variables and measurement ranges are listed in Table 2. In addition, each
 129 test is repeated several times in order to minimise accidental errors, so the average data are
 130 likely to be close to the true values.

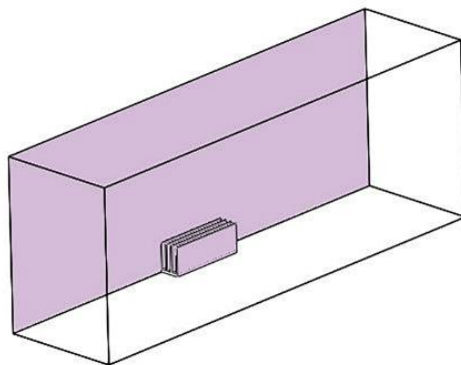
131 **Table 2** Accuracies of sensors and the maximum relative errors of variables

	Temperature		Voltage	Current	Heating power	Thermal resistance
	TC	RTD				
Accuracy	± 0.5°C	± 0.15 °C	± 0.3V	± 0.01A	-	-

Maximum error	1.823%	1.367%	0.411%	0.909%	0.998%	2.08%
---------------	--------	--------	--------	--------	--------	-------

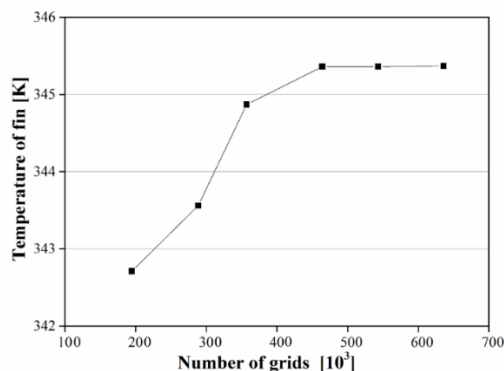
132 **3. Numerical simulation model**

133 The CFD simulation is carried out for the tested straight-fin heatsink using the
 134 symmetric model because the object is symmetric. The simulation zone is shown in Fig. 4 and
 135 its dimension is 900mm×456mm×330mm. Because of the regular geometric shape of the
 136 simulation zone, the hexahedral grid is adopted in the meshing procedure which will not only
 137 get high-quality grid but also be easy to modify the meshing strategy. The mesh density near
 138 the fin surface is increased for its $Y^+ < 1$ [23]. The simulation is carried out with different
 139 meshing strategies, the average surface temperatures of the fin are monitored and compared.
 140 The simulation results are shown in Fig. 5, it can be seen that the optimum meshing strategy is
 141 one with the grid number of 464058, and the optimum mesh model is shown in Fig. 6.



142
143

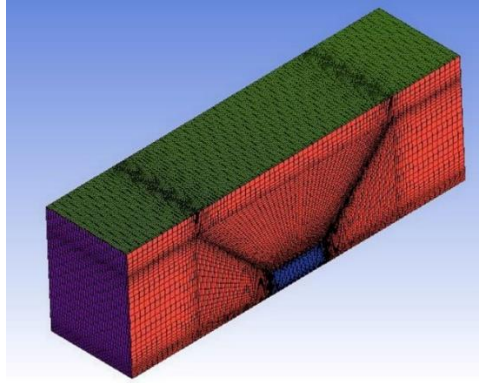
Fig. 4. Scope of the simulation



144

145
146

Fig. 5. Grid independence check



147
148

Fig. 6. Final meshed model

149 In order to reduce the amount of computational resources, the following assumptions

150 are made:

- 151 1) The air flow is treated as a three-dimensional steady laminar flow.
- 152 2) Boussinesq model is used in air zone.
- 153 3) The temperature and heat flow of the heat plate are even.
- 154 4) Except density, the properties of air are constant.
- 155 5) Air is nonslip on the fin surface.
- 156 6) The viscous dissipation and radiation heat transfer are not considered.

157 *3.1. Model for fluid region*

158 Based on the mass conservation principle, the following continuity equation is

159 adopted.

$$\frac{\partial(\rho u)}{\partial x} + \frac{\partial(\rho v)}{\partial y} + \frac{\partial(\rho w)}{\partial z} = 0 \quad (4)$$

161 Where ρ is air density, u , v , w are components of velocity, x , y , z are components of coordinate.

162 Energy equation is obtained on the basis of energy balance characteristics.

163
$$\frac{\partial(\rho u T)}{\partial x} + \frac{\partial(\rho v T)}{\partial y} + \frac{\partial(\rho w T)}{\partial z} = \frac{\kappa}{c_p} \left(\frac{\partial^2 T}{\partial x^2} + \frac{\partial^2 T}{\partial y^2} + \frac{\partial^2 T}{\partial z^2} \right) \quad (5)$$

164 Where T is air temperature, k is air thermal conductivity, C_p is air specific heat
 165 capacity.

166 The natural-convection flow is driven by the air density change and gravity force under
 167 heating condition. For external natural convection flow, the momentum equations can be
 168 written as:

169
$$\frac{\partial(\rho u^2)}{\partial x} + \frac{\partial(\rho uv)}{\partial y} + \frac{\partial(\rho uw)}{\partial z} = -\frac{\partial p}{\partial x} + \mu \left(\frac{\partial^2 u}{\partial x^2} + \frac{\partial^2 u}{\partial y^2} + \frac{\partial^2 u}{\partial z^2} \right) \quad (6)$$

170
$$\frac{\partial(\rho uv)}{\partial x} + \frac{\partial(\rho v^2)}{\partial y} + \frac{\partial(\rho vw)}{\partial z} = -\frac{\partial p}{\partial y} + \mu \left(\frac{\partial^2 v}{\partial x^2} + \frac{\partial^2 v}{\partial y^2} + \frac{\partial^2 v}{\partial z^2} \right) + g(\rho - \rho_0) \quad (7)$$

171
$$\frac{\partial(\rho uw)}{\partial x} + \frac{\partial(\rho vw)}{\partial y} + \frac{\partial(\rho w^2)}{\partial z} = -\frac{\partial p}{\partial z} + \mu \left(\frac{\partial^2 w}{\partial x^2} + \frac{\partial^2 w}{\partial y^2} + \frac{\partial^2 w}{\partial z^2} \right) \quad (8)$$

172 Where p is air static pressure, μ is air viscosity.

173 3.2. Model for solid region

174 There is no internal heat source in the heat sink, so energy equation of solid region
 175 can be written as:

176
$$\frac{\partial^2 T}{\partial x^2} + \frac{\partial^2 T}{\partial y^2} + \frac{\partial^2 T}{\partial z^2} = 0 \quad (9)$$

177 For natural-convection flow, the simulation can get quick convergence with the
 178 Boussinesq model,

179
$$\rho = \rho_0 [1 - \beta(T - T_0)] \quad (10)$$

180 Where ρ is air density at temperature T , ρ_0 is air density at T_0 , β is air thermal expansion
 181 coefficient.

182 The interface between the fluid and solid domains is treated as the fluid-solid coupling
183 surface, and no-slip condition is used for the fluid-solid boundary. The bottom of the heat sink
184 is set as 'WALL' with a constant heat flux.

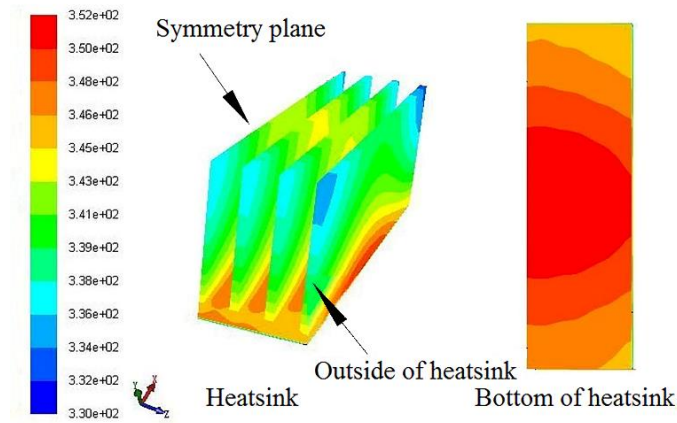
185 Low Reynolds number k- ϵ Turbulent Model is adopted in the simulation program
186 because more accurate results can be obtained compared with the wall function method [24].
187 Especially, it can limit the error no more than 2% when coupled with full pressure outlet
188 boundary condition. The other settings are Pressure based solver, SIMPLE algorithm, PRESTO!
189 (Pressure Staggered Option) for pressure, Second order upwind format for other parameters.
190 The residual value used as convergence indicator is 1e-06. The heat flux at the heat sink bottom
191 and the fin surface temperature are also used as ancillary convergence indicators.

192 **4. Results and discussion**

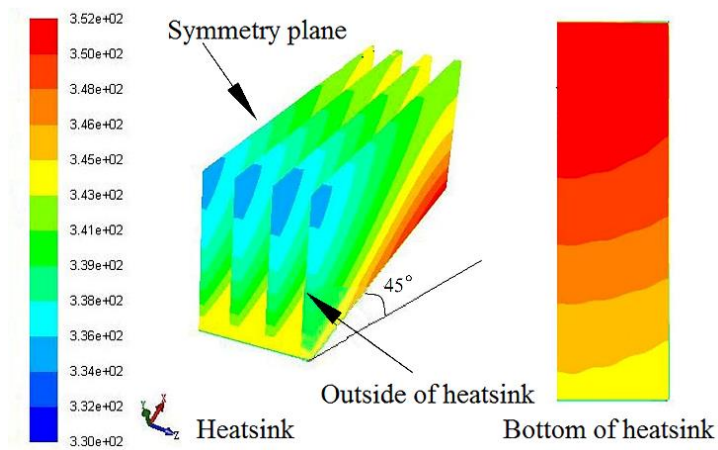
193 *4.1. Temperature distribution of heat sink*

194 The fin temperature measurement results are listed in Table 3 at the mounting angle of
195 0°. It can be found from this table, the fin bottom temperatures (Points 1-6 in Fig. 3) are almost
196 same, but the surface temperatures (Points 7-9 in Fig. 3) are different. The surface temperature
197 at the heat sink centre (Point 8) is obviously higher than those near the heatsink edge. As shown
198 in Fig. 7, the temperature distributions of the heat sink fin and bottom are not uniform whether
199 the mounting angle is 0° or 45°. At the mounting angle of 0°, the highest temperature appears
200 at the heat sink centre while the lowest temperature happens at the fin corner. The fin
201 temperature in the middle of the heatsink is always higher than the others. This is consistent

202 with the experiment results in Table 3. Compared with the mounting angle of 0° , the highest
 203 temperature zone moves to the fin end edge at the mounting angle of 45° .



(a) Mounting angle 0°



(b) Mounting angle 45°

Fig. 7. Temperature contours of fin and bottom of heat sink with mounting angles 0° and 45°

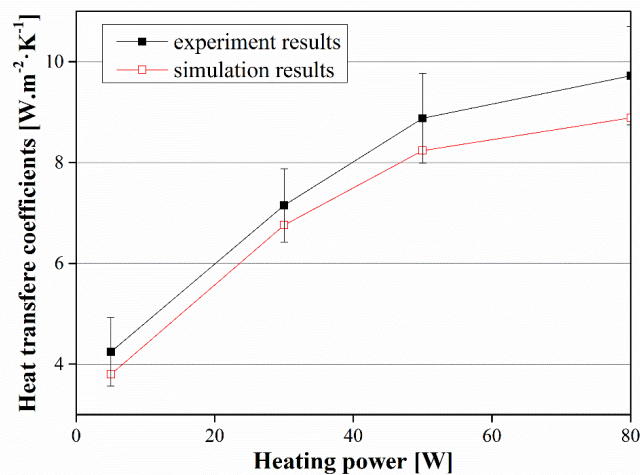
Table 3 Fin temperatures at measuring points

Heating power (W)	Temperature at measuring point ($^\circ\text{C}$)									Average of bottom temperature ($^\circ\text{C}$)
	1	2	3	4	5	6	7	8	9	
5	24	22	24	24	23	22	17	20	18	23.2
10	33	35	35	34	34	34	30	33	30	34.2

20	47	48	46	47	47	47	41	45	42	47
30	52	53	53	51	52	52	48	50	47	52.2
40	62	61	61	61	62	63	57	60	55	61.7
50	67	68	67	67	70	70	64	69	64	68.2
60	82	80	80	80	84	83	72	76	74	81.5
70	87	88	86	86	87	88	81	84	82	87
80	92	92	92	93	94	94	86	91	85	92.8

212 4.2. Influence of heating power on heat transfer coefficient

213 Heat transfer coefficients from simulation and experimental test are shown in Fig. 8 at
214 the heat sink mounting angle of 0°. It is found that the variation of simulation data is similar to
215 that of experiment results. The maximum error between them is about 10.5% which is
216 acceptable. Heat transfer coefficient increases rapidly with the heating power when the heating
217 power is below 50W, but it increases moderately when the heating power is over 50W. The
218 heat transfer driving force in the heat sink is the air flow, the air will get more heat from the
219 heat sink as the heating power increases, and its flow velocity will increase as well, so the heat
220 transfer coefficient becomes higher. The air flow resistance, however, will increase with the
221 velocity, therefore the increase rate of heat transfer coefficient will decrease synchronously.

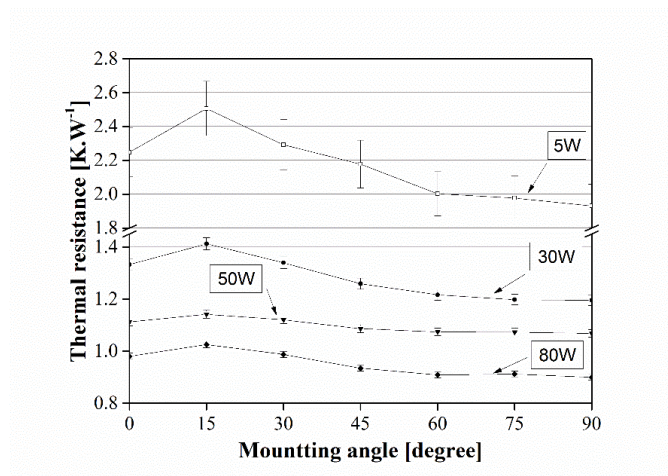


222
223

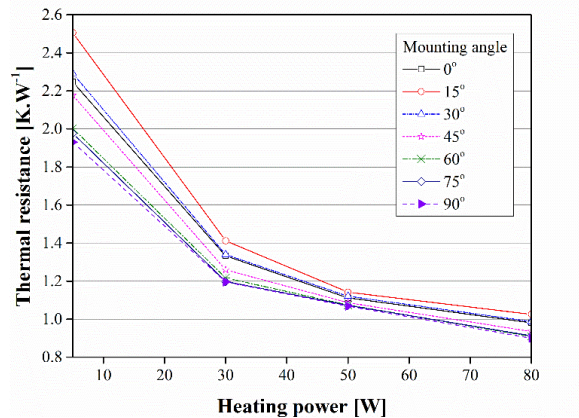
Fig. 8. Experimental and simulation results of heat transfer coefficient

224 4.3. Influences of heating power and mounting angle on thermal resistance

225 The variation of thermal resistance with the mounting angle is shown in Fig. 9. The
226 thermal resistance increases with the mounting angle at first and reaches the maximum when
227 the mounting angle is 15°, then it decreases. The variation of thermal resistance is not
228 significant when the mounting angle is over 60°, it reaches the minimum when the mounting
229 angle is 90°. When heating power is higher than 50W, the fluctuation of thermal resistance is
230 moderate, especially there is nearly no variation when the mounting angle is bigger than 60°.
231 The ratios between the maximum and minimum thermal resistances for the heating powers of
232 5W, 30W, 50W and 80W, are 29.78%, 18.12%, 6.88% and 13.98% respectively. So in practice,
233 the mounting angle should be set as 90°. The variation of thermal resistance with heating power
234 is shown in Fig. 10. It is found that thermal resistance decreases with heating power. Thermal
235 resistances at the mounting angle of 15° are the biggest for all heating powers, while the
236 resistances are the smallest and have no obviously different when the mounting angles are 60°,
237 75°, and 90°.



238
239 **Fig. 9.** Thermal resistance variation with mounting angle (experimental results)
240

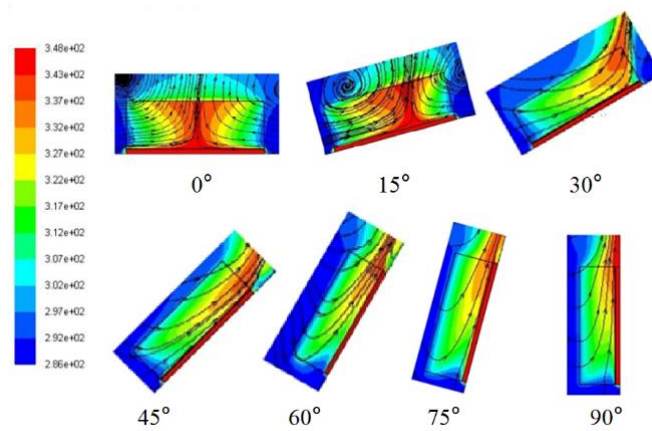


241
242 **Fig. 10.** Thermal resistance variation with heating power (experimental results)

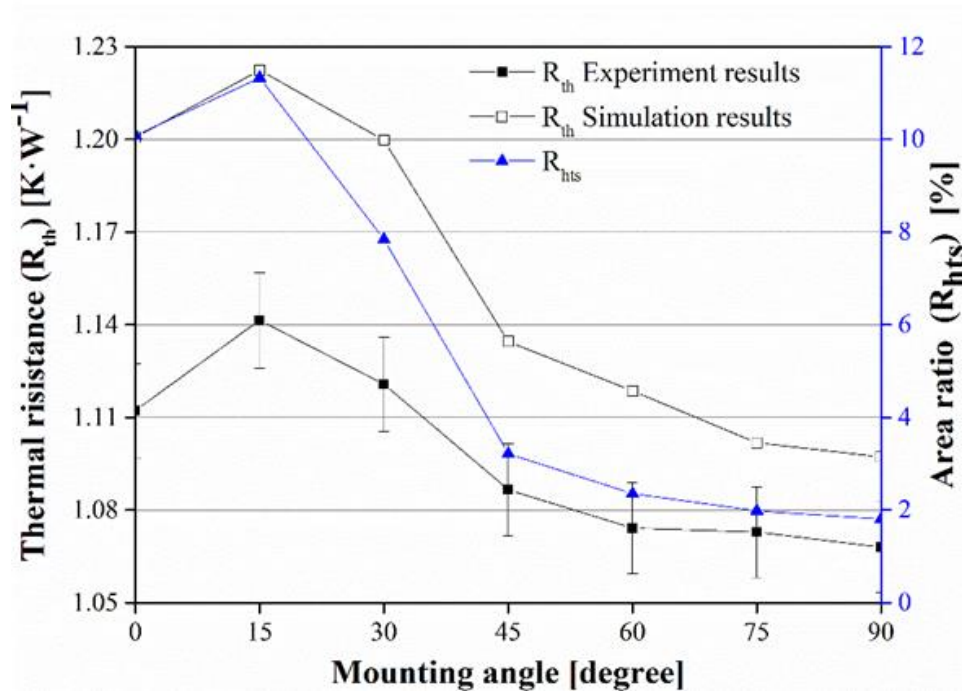
243 *4.4. Fluid temperature distribution and thermal resistance*

244 Air streamlines and temperature distribution between the fins under 50W heating power
 245 condition are shown in Fig. 11. The variation of temperature contour has relevance to the fluid
 246 flow. The air flow direction moves to the upper side of the heat sink when the mounting angle
 247 increases. The position of the high-temperature zone changes following the fluid flow direction.
 248 The highest temperature always appears at the zone where the air flows out of the heat sink.
 249 The red zone in Fig. 11 represents that the air temperature is in the range from 70°C to 75°C.
 250 According to Fig. 7, the fin surface temperature at one zone is in the same range because of
 251 high thermal conductivity of the heat sink material, which means that the temperature
 252 difference between the fin and airflow is less than 5°C in this zone, calling it ‘D zone’ for easy
 253 identification. It also can be seen from Fig. 7 and Fig. 11 that in the other zones, the temperature
 254 difference between the fin and airflow is larger than 30°C, calling it ‘A zone’. According to
 255 heat transfer equation $Q=hA\Delta T$, ΔT will be the key factor when h is kept constant or slightly
 256 fluctuate. Therefore, heat transfer in the ‘D zone’ will be very small compared to that in the ‘A
 257 zone’ and even can be ignored, so the ‘D zone’ is named as ‘heat transfer stagnation zone’. The

258 bigger the area of heat transfer stagnation zone, the lower the heat transfer. Then the area ratio
 259 (R_{hts}) of heat transfer stagnation zone to the fin is assessed. Fig. 12 shows R_{hts} variation with
 260 the mounting angle. It is found that the R_{hts} variation is similar to that of thermal resistance.
 261 They reach the maximum values at the mounting angle of 15° . The R_{hts} increases at first and
 262 then decrease sharply, afterwards it declines mildly. Fig. 12 confirms that the heat transfer
 263 stagnation zone is the main factor influencing the heat sink performance.



264 **Fig. 11.** Streamlines and temperature contours at different mounting angles
 265



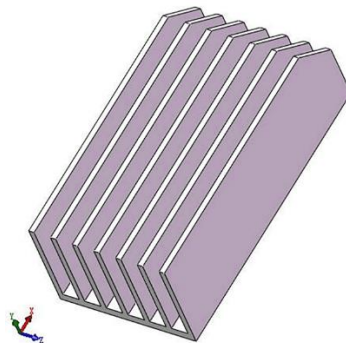
266

267 **Fig. 12.** Thermal resistance (R_{th}) and area ratio (R_{hts}) variations with mounting angle at 50W heating power

268 4.5. *Cutting effect*

269 The area and location of red zone change with the mounting angle as shown in Fig. 11.
270 The location of red zone is just at the corner of the fin when the mounting angle is 30° , so
271 cutting this corner would decrease thermal resistance, this will confirm the inference that the
272 heat transfer stagnation zone is the main aspect to affect the heat sink performance. Another
273 reason for cutting this corner is that there is less influence on original air flow.

274 The new heat sink is shown in Fig. 13. The size of the cut corner is $20\text{mm}\times 20\text{mm}$, the
275 cut area takes up 2.5% of the whole fin area. The experimental results of the new heat sink at
276 50W and 80W heating powers are indicated in Fig. 14 and Fig. 15. It is found from Fig. 14 that
277 the thermal resistance reduces about 2.64%~3.77% at heating power of 50W and 6.00%~10.13%
278 at heating power of 80W. It is also found from Fig. 15 that the heat transfer coefficient increases
279 about 7.30%~10.77% at heating power of 50W and 11.46%~17.07% at heating power of 80W.
280 The variations of thermal resistance at the mounting angles of 0° , 15° and 30° are smaller than
281 those under other mounting angles. According to Fig. 11, this is in line with the previous
282 assumption because the heat transfer stagnation zone is located at the fin corner.



283
284

Fig. 13. 3D drawing of cut corner heat sink

285
286
287

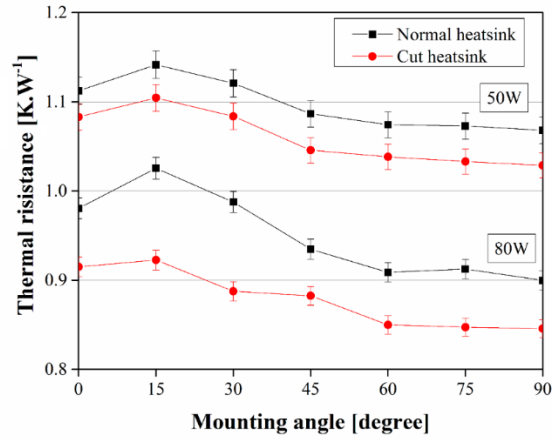
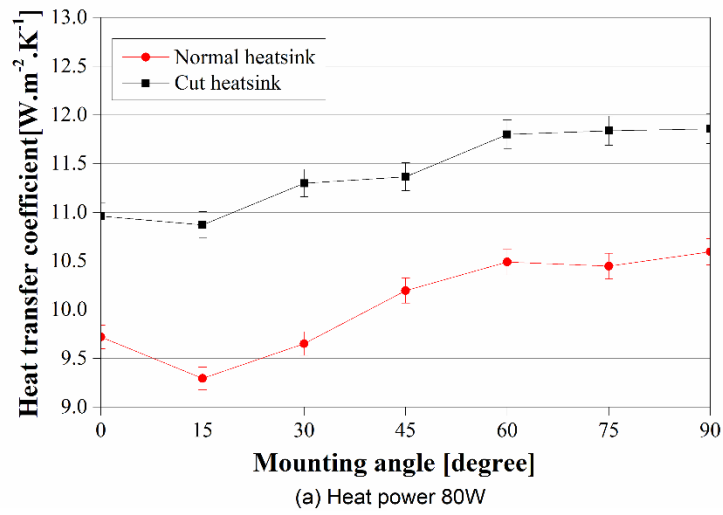
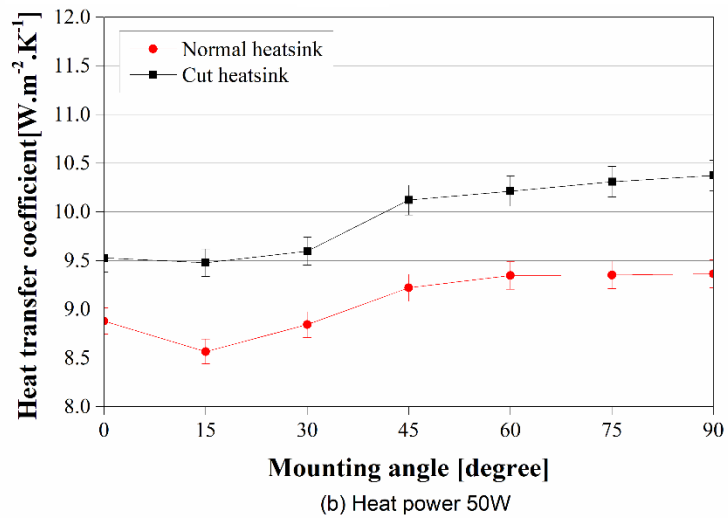


Fig. 14. Thermal resistance variation with mounting angle



(a) Heat power 80W



(b) Heat power 50W

288
289
290

Fig. 15. Heat transfer coefficients at different mounting angles

291 **5 Conclusion**

292 Heat transfers of a straight fin heat sink under natural convection condition are
293 investigated at different mounting angles in this paper. The heat sink surface temperatures are
294 measured and used to judge its performance under constant heating power condition. The
295 simulation results are verified by the experimental data with the maximum error less than
296 10.5%. The heat sink performance is the worst at the mounting angle of 15°, and the best
297 performance happens at the angle of 90°. The heat transfer stagnation zone is identified where
298 the temperature difference is less than 2°C in this study. The heat transfer stagnation zone area
299 reaches the maximum when the mounting angle is 15°, that leads to the lowest performance
300 because the effective heat dissipation area of the heatsink is the smallest. This is verified by
301 cutting the corner portion of the heat sink where is the heat transfer stagnation zone. The heat
302 transfer could be enhanced by cutting appropriate corner of the heat sink, the thermal resistance
303 reduces 2.64%~3.77% at heating power of 50W and 6.00%~10.13% at heating power of 80W,
304 and heat transfer coefficient increases 7.30%~10.77% at heating power of 50W and
305 11.46%~17.07% at heating power of 80W.

306

307 **Conflict of interest**

308 The authors declared that there is no conflict of interest.

309

310 **Acknowledgements**

311 Part of the work presented in this paper has received funding from the Scientific and
312 Technological Planning Projects of Henan Province, China (No.162102310504). A part of this
313 work was supported by the Foundation of State Key Laboratory of Coal Combustion
314 (No.FSKLCC1410). The financial support is gratefully acknowledged.

315 **Nomenclature**

- 316 A heat sink surface area, m^2
- 317 c_p specific heat capacity of fluid, $J.kg^{-1}.K^{-1}$
- 318 h heat transfer coefficient, $W.m^{-2}.K^{-1}$
- 319 k thermal conductivity, $W.m^{-1}.K^{-1}$
- 320 Q_{hs} heatsink input power, W
- 321 R_{th} thermal resistance, $K.W^{-1}$
- 322 R_{hts} the ratio of stagnation zone accounts for the fin whole area, dimensionless
- 323 T_{ave} average temperature of heat sink plate, K
- 324 T_{am} ambient temperature, K
- 325 ΔT temperature difference between heat sink surface and the ambient temperature, K
- 326 u, v, w components of velocity, $m.s^{-1}$
- 327 x, y, z components of coordinate
- 328 $x_1, x_2, x_3, \dots, x_n$ independent variables
- 329 $\delta x_1, \delta x_2, \delta x_3 \dots \delta x_n$ errors of independent variables
- 330 *Greek Symbols*

331 β thermal expansion coefficient, K^{-1}

332 ρ air density, $kg.m^{-3}$

333 ρ_0 air density at T_0 , $kg.m^{-3}$

334 μ viscosity, $N.s.m^{-2}$

335

336

337 **References**

338 [1]. S. Belhardj, S. Mimouni, A. Saidane, M. Benzohra, Using microchannels to cool
339 microprocessors: a transmission-line-matrix study, *Microelectron J.* 34(4)(2003), 247-
340 253.

341 [2]. H. Daniel, S. Bartolome, Y. Ryo, U. Satoshi, Y. Masafumi, K. Lars, S. Hiroshi, U.
342 Satoshi, Liquid-Crystalline Dye-Sensitized Solar Cells: Design of Two-Dimensional
343 Molecular Assemblies for Efficient Ion Transport and Thermal Stability, *Chemistry of*
344 *Materials* 28(18)(2016) 6493-6500.

345 [3]. W. Elenbaas, Heat dissipation of parallel plates by free convection, *Physica* 9(1)(1942)
346 1-28.

347 [4]. J. R Bodoia, J. F. Osterle, The development of free convection between heated vertical
348 plates, *J. Heat Transf.* 84(1) (1962) 40-43.

349 [5]. C. D Jones, L. F. Smith, Optimum Arrangement of Rectangular Fins on Horizontal
350 Surfaces for Free-Convection Heat Transfer, *Journal of Heat Transfer-Transactions*
351 *ASME* 92 (1) (1970) 6-10.

- 352 [6]. B. Yazicioğlu, H. Yüncü, Optimum fin spacing of rectangular fins on a vertical base in
353 free convection heat transfer, *Heat Mass Transfer*. 44(1) (2007) 11-21.
- 354 [7]. H. K. Tae, H. D. Kyu, K. K. Dong, Closed form correlations for thermal optimization
355 of plate-fin heat sinks under natural convection, *Int. J. Heat Mass Transf.* 54(5-6) (2011)
356 1210-1216.
- 357 [8]. J., Zhou, C., Yang, L. Zhang, Minimizing the entropy generation rate of the plate-
358 finned heat sinks using computational fluid dynamics and combined optimization, *Appl.*
359 *Therm. Eng.* 29 (8-9) (2009) 1872-1879.
- 360 [9]. S. Yu, K. Lee, S. Yook, Natural convection around a radial heat sink, *Int. J. Heat Mass*
361 *Transf.* 53(13-14) (2010) 2935-2938.
- 362 [10]. S. Yu, K. Lee, S. Yook, Optimum design of a radial heat sink under natural convection,
363 *Int. J. Heat and Mass Transf.* 54 (11-12) (2011) 2499-2505.
- 364 [11]. D. Jang, S. Yook, K. Lee, Optimum design of a radial heat sink with a fin-height profile
365 for high-power LED lighting applications, *Appl. Energy* 116 (2014) 260-268.
- 366 [12]. M. A. Ismail, M. Z. Abdullah, M. A. Mujeebu, A CFD-based experimental analysis on
367 the effect of free stream cooling on the performance of micro processor heat sinks, *Int.*
368 *Commun. Heat and Mass Transf.* 35 (6) (2008) 771-778.
- 369 [13]. X. Yu, J. Feng, Q. Feng, Q. Wang, Development of a plate-pin fin heat sink and its
370 performance comparisons with a plate fin heat sink, *Appl. Therm. Eng.* 25 (2-3) (2005)
371 173-182.

- 372 [14]. G. Huang, S. Wong, C. Lin, Enhancement of natural convection heat transfer from
373 horizontal rectangular fin arrays with perforations in fin base, *Int. J. Therm. Sci.* (84)
374 (2014) 164-174 .
- 375 [15]. M. Ahmadi, G. Mostafavi, M. Bahrami, Natural convection from rectangular
376 interrupted fins, *Int. J. Therm. Sci.* (82) (2014) 62-71.
- 377 [16]. M. R. Shaeri, M. Yaghoubi, Thermal enhancement from heat sinks by using perforated
378 fins, *Energy Convers. Manage.* 50 (5) (2009) 1264-1270.
- 379 [17]. D. S. Mangesh, M. Ashish, Natural convection heat transfer from a radial heat sink with
380 horizontal rectangular fins, *Int. J. Innovat. Res. Adv. Eng.* 1(8) (2014) 353-356
- 381 [18]. R. G. Hamid, F. Mahdi, Mohammad M. N., Improvement of free convection heat
382 transfer rate of rectangular heatsink on vertical Base plates. *Energy and Power Eng.*, (3)
383 (2011) 525-532.
- 384 [19]. M. Mehrtash, I. Tari, A correlation for natural convection heat transfer from inclined
385 plate-finned heat sinks, *Appl. Therm. Eng.* 51(1-2) (2013) 1067-1075
- 386 [20]. I. Tari, M. Mehrtash, Natural convection heat transfer from horizontal and slightly
387 inclined plate-fin heat sinks, *Appl. Therm. Eng.* 61(2) (2013) 728-736.
- 388 [21]. I. Tari, M. Mehrtash, Natural convection heat transfer from inclined plate-fin heat sinks,
389 *Int. J. Heat Mass Transf.* 56 (1-2) (2013) 574-593.
- 390 [22]. Q. Shen, D. Sun, Y. Xu, T. Jin, X. Zhao, Orientation effects on natural convection heat
391 dissipation of rectangular fin heat sinks mounted on LEDs, *Int. J. Heat Mass Transf.* 75
392 (2014) 462-469.

393 [23]. M. S. Salim, C. C. Siew, Wall y^+ strategy for dealing with wall-bounded turbulent,
394 IMECS 2009, Hong Kong, China, 2009, 2165-2170.

395 [24]. A. Mohd, M. S. Salim, C. C. Siew , Wall y^+ approach for dealing with turbulent flow
396 over a surface mounted cube: Part1-Low Reynolds Number, 7th International Conf. on
397 CFD in the Minerals and Process Industries CSIRO, Melbourne, Australia, 2009,1-6.

398